α-Fluorophosphonates reveal how a phosphomutase conserves transition state conformation over hexose recognition in its two-step reaction

Yi Jin[a,1], Debabrata Bhattasali[b,1], Erika Pellegrini[a,c,d,1], Stephanie M. Forget[b], Nicola J. Baxter[a], Matthew J. Cliff[a,e], Matthew W. Bowler[c,d,f], David L. Jakeman[b,2], G. Michael Blackburn[a,2] and Jonathan P. Waltho[a,e,2]

Supporting Information

Chemical synthesis. A complete description of the synthesis and characterization of compounds βG1CF$_S$P (**1a**) and βG1CF$_R$P (**2a**) is provided in the **General methods for synthesis.**

Potentiometric titration. pK_a values were measured using an IQ Scientific Instruments IQ150 fitted with an ISFET probe. A 0.01 M solution of the diammonium phosphonate salt was adjusted to pH 10.0 with 0.2 M NaOH and titrated with 5 μL aliquots of 0.2 M HCl to pH 2.0. Data were recorded according to previous methods, and pK_a values were determined by plotting in GraFit 5.0.4 (Erithacus Software Limited) (39).

Protein production and purification. Production and purification of *Lactococcus lactis* βPGM was carried out using *E. coli* BL21(DE3) as described previously (4).

NMR spectroscopy. 1D ^{1}H and ^{19}F NMR spectra were recorded at 298 K on a Bruker Avance 500 MHz spectrometer (operating at 470.38 MHz for fluorine) equipped with a 5 mm QXI probe equipped with *z*-axis gradients. Integration of peaks was performed using FELIX (Felix NMR, Inc. San Diego, CA), with phase adjustment and baseline correction optimized for the chosen peaks. Indirect referencing of ^{19}F chemical shifts was achieved by using gyromagnetic ratios: ^{19}F/^{1}H = 0.940940080. Solvent-induced isotope shifts (SIIS) on the ^{19}F resonances were measured by comparing spectra for samples separately prepared in 50 mM K^+ HEPES buffer pH 7.2 containing either 10% D_2O or 100% D_2O and are defined as $[\delta^{19}F_{(H2O\ buffer)} - \delta^{19}F_{(100\%\ D2O\ buffer)}]$.

Relative dissociation constants for the AlF_4^- TSA complexes of βG1P and G6P were also measured by ^{19}F NMR. The sample contained 1.0 mM βPGM, 5 mM $MgCl_2$, 2 mM $AlCl_3$, 20 mM NH_4F and 10% D_2O in 50 mM K^+ HEPES (pH 7.2) with 5 mM G6P and 25 mM βG1P present at 298 K. Under these enzyme-saturating conditions, the ratio of the ^{19}F resonances for the two TSA complexes [βPGM-AlF_4^--G6P]/[βPGM-AlF_4^--βG1P] = 1.0 and $K = K_{dG6P}/K_{dG1P}$ = [βPGM-AlF_4^--G6P][βG1P]/[βPGM-AlF_4^--βG1P][G6P] = 5.4. The binding energy difference of these two TSA complexes relative to the free sugar phosphates is RTln$K$ = 4.2 kJ mol^{-1}. The intrinsic equilibrium constant (14) for G6P:βG1P is ~30, corresponding to 8.4 kJ mol^{-1}, giving a total binding energy difference for TSA complex formation of 12.6 kJ mol^{-1}. NMR experiments were completed within 30 min to minimize changes in the sugar phosphate concentrations resulting from any residual enzyme activity.

Fluorescence titration. Fluorescence titration measurements to determine the apparent dissociation constants for sugar phosphate / sugar phosphonate ligands with βPGM were performed at 295 K using a Cary Eclipse spectrofluorimeter in 1.4 mL fluorimetry quartz cuvettes (Hellma). βPGM was diluted to a final concentration of 10 or 20 μM in 50 mM K^+ HEPES pH 7.2, 5 mM $MgCl_2$, 1 mM EDTA and 10 mM NH_4F. The reaction mixture was

serially titrated with aliquots of 1 mM, 5 mM, and 50 mM ligand stock using the same buffer as for the protein sample. After each addition of ligand, the sample was thoroughly mixed by pipetting. An excitation wavelength of 285 nm was used and emission spectra in the range of 300 to 400 nm were collected. The fluorescence intensity at 325 nm was used in the apparent K_d calculations. Due to a trace impurity in βG1CP, a correction for the absorption of the excitation beam by the filter effect was carried out before the calculation. Experiments were repeated in triplicate before averaging.

Origin8^{TM} was used for fitting the results according to the equation: $y = F_0 + \Delta F \times x / (K_d + x)$ for tight binding, or $y = F_0 + \Delta F$ (P + K_d + x − $\sqrt[2]{(\mathbf{P} + \boldsymbol{K}\mathbf{d} + \boldsymbol{x})^2 - 4\mathbf{P}\boldsymbol{x}}$)/2P for weak binding, where $y = F_{325nm}$ × dilution factor. F_{max} is the fluorescence observed at ligand concentration x μM, F_0 is the fluorescence of the apo-protein before addition of ligand, and P is the total protein concentration. The two variable parameters are the dissociation constant K_d and maximum fluorescence change $\Delta F = F_{max} - F_0$. It proved not possible to determine K_d values for βG1P or G6P for trifluoromagnesate TSA complex formation as these substrates turned over during the course of the measurements. Titration experiments for the compounds in AlF_4^- TSA complexes were carried out using the same method but with the supplement of 1 mM $AlCl_3$ to both protein buffers and ligand stocks.

X-ray crystallography. Crystallization of TSA complexes for the methylenephosphonate analog βPGM-MgF_3^--βG1CP (4C4R), for the monofluoromethylenephosphonate analog βPGM-MgF_3^--βG1CF_SP, (4C4S) and βPGM-AlF_4^--βG1CF_SP (4C4T), were carried out as previously described (4). Buffer was freshly exchanged to 50 mM K^+ HEPES pH 7.2, 5 mM $MgCl_2$ and 0.1 mM DTT prior to the crystallization experiments. For each complex, 10 mM NH_4F and 5 mM βG1P analog were added at a protein concentration of 15 mg mL^{-1}. For the βPGM-AlF_4^--βG1CF_SP TSA complex, a further 2 mM $AlCl_3$ was added. For crystallization, 2 μL of the complex solution defined above was mixed 1:1 with the precipitant (27~32% PEG 4000, and 50~75 mM magnesium acetate) and placed in sitting-drop crystallization plates. Large plate crystals appeared between overnight and a few days. They were mounted directly from the mother liquor using a mesh loop and cryocooling as described (40). For crystallization of the 6-phosphonomethylene-6-deoxyglucopyranose (G6CP) complex, 2 μl of the AlF_4^- inhibited protein containing 10 mM G6CP was mixed 1:1 with the precipitant (19-21% PEG 3350 and 50 mM magnesium acetate) and placed in sitting drop crystallization plates. Large plate crystals appeared after one week and had the approximate dimensions 0.5 mm × 0.1 mm × 0.1 mm. For cryoprotection, the crystals were transferred to a buffer containing 22% PEG 3350, 50 mM magnesium acetate, 2 mM $AlCl_3$, 10 mM NH_4F, 10 mM G6CP, 5 mM $MgCl_2$, 50 mM K^+ HEPES pH 7.2 and 5% PEG 400 (v/v). The PEG 400 concentration was increased to 20% (v/v) in 5% steps (15 min at each concentration) by transferring the crystals between buffers with an increasing concentration of PEG 400. Crystals were harvested with a mounted LithoLoop (Molecular Dimensions Ltd., Newmarket, UK), plunged into liquid nitrogen and stored at 100 K.

Diffraction data collection and refinement method. Diffraction data were collected from cryocooled crystals between 1.5 Å and 1.05 Å resolution (**Table S1**) on a PILATUS 6M detector on beamline ID29 or an ADSC Q4 CCD detector on beamline ID14-2 with a GRob goniometer at the European Synchrotron Radiation Facility, Grenoble, France (41). Data were processed with XDS (42) and programs from the Collaborative Computational

Project Number 4 suite. Structures were solved by molecular replacement with MolRep (43), using the βPGM-MgF_3^--G6P complex as a search model (2WF5) (4), with all ligands and water molecules removed. Refinement was carried out alternately with REFMAC5 (44) and by manual rebuilding with the program COOT (45). Solvent molecules were built with the ARP/waters function of ARP/wARP (46). Ligands were included in the final rounds of refinement. The high resolution of the data led to excellent electron density for the ligands. A refinement dictionary for each molecule was generated using ProDRG (47). The final refinement cycles were carried out using PHENIX refine (48,49). Model validation was performed using MolProbity (50). All complexes crystallized in the orthorhombic space group $P2_12_12_1$ with one molecule in the asymmetric unit. Data collection and refinement statistics are summarized in **Table S1**. Figures were produced with the PyMOL Molecular Graphics System, Version 1.5.0.4 Schrödinger, LLC. Hydrogen bond distances were also measured using PyMOL and all those reported below have angles above 145 °.

Structure analysis of the βG1CF$_S$P, βG1CP, and G6CP TSA complexes. The βPGM-MgF_3^--βG1CP TSA complex (**4C4R)** has a tbp trifluoromagnesate core mimicking the transition state phosphoryl group (4), with coordinating axial ligands comprising glucose-O6 (2.2 Å) and Asp8 Oδ (2.0 Å) at an axial O_{ax}–Mg–O_{ax} angle of 176°, and with Mg–F bonds of 1.8 Å (4). The three equatorial fluorides, that mimic the three equatorial phosphoryl oxygens atoms, are coordinated as follows: F_A to Leu9 N^H (3.0 Å), Asp10 N^H (2.8 Å) and Ser114 O^Hδ (2.6 Å), F_B to Ala115 N^H (2.9 Å) and Lys145 N^Hζ (2.8 Å), and F_C to the catalytic magnesium (2.0 Å). The catalytic magnesium is octahedral, liganded by Asp8 Oδ′, the backbone carbonyl of Asp10, Asp170 Oδ, F_C, and two water molecules **(Fig. S3*A*)**. The nucleophilic 6-OH group is hydrogen bonded to the catalytic aspartate Asp10 Oδ (2.7 Å), in a pseudo-tetrahedral arrangement. The phosphonate moiety in the inert phosphate binding site coordinates to Arg49 N^Hε (2.8 Å) and N^Hη (3.0 Å), Ser116 Oδ (2.5 Å), Lys117 N^H (3.0 Å) and Asn118 N^Hδ (3.1 Å), forming 5 intermolecular hydrogen bonds and having a sixth hydrogen bond to the 2-OH group (2.9 Å). The C7 methylene carbon is 3.4 Å from the nearest neighboring water molecule and is in a staggered conformation with the phosphonate oxygen atoms while the P–C7 bond eclipses H1 on the glucopyranose ring (dihedral angle –10 °; **Fig. S4*D***). The pyranose ring has an undistorted $^4C_1$ chair form. Its three equatorial pyranose hydroxyls form 6 hydrogen bonds directly to amino acid residues: the 2-OH group to Lys76 Nε (3.0 Å), and a phosphonate oxygen (2.9 Å), the 3-OH group to Trp24 Nε (2.9 Å), Leu44 CO (3.3 Å), and Ser52 Oδ (2.9 Å), and the 4-OH group to Leu44 CO (2.8 Å), Gly46 N^H (3.3 Å) and a water molecule (2.7 Å). The pyranose oxygen is not hydrogen bonded but is in van der Waals contact with Ala115 and Ser116, which flank the pyranose core site on one side. The pyranose core site is also capped by the imidazole ring of His20, which is close to the three axial hydrogen atoms on the α-face of the pyranose ring. The β-face of the ring is capped primarily by five amino acid residues, located in the Leu44 to Ser52 loop between helices 2 and 3 in the cap domain (14) (**Fig. S5*A***).

The βPGM-MgF_3^--βG1CF$_S$P TSA complex (**4C4S**) confirms the (*S*)-configuration for the C7-fluorine and aligns well with the corresponding structure for βG1CP (average pairwise rmsd for Cα atoms is 0.086 Å). It makes the same hydrogen bond interactions to the same protein residues. However, C7 is shifted 0.3 Å relative to its position in

βG1CP (**Fig. S4*A***), and its attached fluorine does not make any hydrogen bonds, being 3.3 Å from the nearest water, 3.2 Å from O2, and 2.6 Å from the backbone amide hydrogen of Arg49.

The βPGM-AlF_4^--βG1CF_SP TSA complex (**4C4T)** aligns well with the above two structures (average pairwise rmsd for Cα atoms is 0.075 Å when compared with the βPGM-MgF_3^--βG1CF_SP TSA complex). It has an octahedral AlF_4^- core with two axial ligands O6 (2.0 Å) and Asp8 Oδ (1.9 Å) at an O_{ax}–Al–O_{ax} angle of 175˚ (**Fig. S3*C*)**. The four equatorial fluorides have Al–F bond lengths of 1.8 Å, four F–Al–F bond angles in the range 88˚ to 93˚, and with F_D coordinating the catalytic magnesium (**Fig. S3*F*)**. As for the MgF_3^- complex, the C7-fluorine in the βPGM-AlF_4^- -βG1CF_SP complex is too distant (2.6 Å) from any hydrogen atom to form a hydrogen bond. In both metal fluoride TSA complexes, the C1–C7 bond has rotated to reduce the eclipsed interaction between the C7-fluorine and C2 (giving a separation of 2.9 Å), while maintaining a separation of 3.0 Å between the C7-fluorine and O5 (**Fig. S4*B***).

The βPGM-AlF_4^--G6CP TSA complex (**2WF7**) aligns well with the βPGM-AlF_4^--G6P TSA complex (PDB 2WF6) (average pairwise rmsd for Cα atoms is 0.096 Å). It has an octahedral AlF_4^- core with two axial ligands O6 (2.0 Å) and Asp8 Oδ (1.9 Å) at an O–Al–O angle of 172.5˚. The four equatorial fluorides have Al–F bond lengths of 1.8 Å, four F_{eq}–Al–F_{eq} bond angles in the range 87˚ to 93˚, and with F_D coordinating the catalytic magnesium (**Fig. S3*D***). The four equatorial fluorides are coordinated as follows: F_A to Ala115 N^H (2.7 Å) and Lys145 $N^H\zeta$ (2.8 Å), F_B to Asp10 N^H (2.8 Å), Leu9 N^H (2.9 Å), and Ser114 $O^H\delta$ (2.8 Å), F_C to Lys145 $N^H\zeta$ (3.1 Å), glucose 2-OH (3.1 Å), and a water ligand of the catalytic magnesium (2.6 Å), and F_D to glucose 2-OH (2.8 Å) and the catalytic magnesium (2.0 Å). The catalytic magnesium is octahedral, liganded by Asp8 Oδ′ (2.1 Å), the backbone carbonyl of Asp10 (2.1 Å), Asp170 Oδ (2.0 Å), F_C, and two water molecules. The nucleophilic 1-OH group is hydrogen bonded to the catalytic aspartate Asp10 Oδ (2.6 Å), in a pseudo-tetrahedral arrangement (**Fig. S3*D***). The 6-methylenephosphonate moiety in the inert phosphate binding site coordinates to Arg49 $N^H\varepsilon$ (2.8 Å) and $N^H\eta$ (3.3 Å), Asn118 $N^H\delta$ (2.8 Å), Ser116 Oδ (2.6 Å), and Lys117 N^H (2.9 Å), forming 5 intermolecular hydrogen bonds and having a sixth hydrogen bond to a water (2.8 Å).

39. Huestis MP, Aish GA, Hui JPM, Soo EC, Jakeman DL (2008) Lipophilic sugar nucleotide synthesis by structure-based design of nucleotidylyltransferase substrates. *Org Biomol Chem* 6(3):477-484.

40. Pellegrini E, Piano D, Bowler MW (2011) Direct cryocooling of naked crystals: are cryoprotection agents always necessary? *Acta Cryst D* 67(10):902-906.

41. Ferrer JL, Larive NA, Bowler MW, Nurizzo D (2013) Recent progress in robot-based systems for crystallography and their contribution to drug discovery. *Expert Opin Drug Discov* 8(7):835-847.

42. Kabsch W (2010) XDS. *Acta Cryst D* 66(2):125-132.

43. Vagin A, Teplyakov A (2010) Molecular replacement with MOLREP. *Acta Cryst D* 66(1):22-25.

44. Murshudov GN, Vagin AA, Dodson EJ (1997) Refinement of macromolecular structures by the maximum-likelihood method. *Acta Cryst D* 53(3):240-255.

45. Emsley P, Cowtan K (2004) Coot: model-building tools for molecular graphics. *Acta Cryst D* 60(12):2126-2132.

46. Lamzin VS, Wilson KS (1993) Automated refinement of protein models. *Acta Cryst D* 49(1):129-147.

47. Schuttelkopf AW, van Aalten DM (2004) PRODRG: a tool for high-throughput crystallography of protein-ligand complexes. *Acta Cryst D* 60(8):1355-1363.

48. Afonine PV et al. (2012) Towards automated crystallographic structure refinement with PHENIX refine. *Acta Cryst D* 68(4):352-367.

49. Adams PD et al. (2010) PHENIX: a comprehensive Python-based system for macromolecular structure solution. *Acta Cryst D* 66(2):213-221.

50. Chen VB et al. (2010) MolProbity: all-atom structure validation for macromolecular crystallography. *Acta Cryst D* 66(1):2-21.

51. Blackburn GM, Bowler MW, Jin Y, Waltho JP (2012) Reflections on biocatalysis involving phosphorus. *Biochemistry (Moscow)* 77(10):1083-1096.

Table S1. Data collection and refinement statistics.

	βPGM-MgF_3^--βG1CF$_S$P	βPGM-AlF_4^--βG1CF$_S$P	βPGM-MgF_3^--βG1CP	βPGM-AlF_4^--G6CP
PDB Code	**4C4S**	**4C4T**	**4C4R**	**2WF7**
Data collection				
Space group	$P2_12_12_1$	$P2_12_12_1$	$P2_12_12_1$	$P2_12_12_1$
Cell dimensions				
a, *b*, *c* (Å)	37.54, 54.34, 104.35	37.19, 54.28, 104.5	38.01, 54.20, 105.41	37.5, 54.3, 104.7
α, β, γ (°)	90.0, 90.0, 90.0	90.0, 90.0, 90.0	90.0, 90.0, 90.0	90.0, 90.0, 90.0
Resolution (Å)	20-1.5 (1.58-1.5)	20-1.5 (1.58-1.5)	20-1.1 (1.16-1.1)	20-1.05 (1.11-1.05)
R_{merge}	0.042 (0.338)	0.085 (0.595)	0.052 (0.352)	0.06 (0.22)
I / σI	19.8 (3.2)	12.5 (2.1)	12.7 (4.9)	7.6 (1.6)
Completeness (%)	97.1 (88.1)	98.1 (92.1)	93.1 (85.7)	89.2 (55.0)
Redundancy	3.4 (2.9)	4.2 (3.4)	4.7 (4.7)	2.3 (1.3)
Refinement				
Resolution (Å)	20-1.5	20-1.5	20-1.1	20-1.05
No. reflections	33872	34022	82900	89213
R_{work} / R_{free}	17.3/19.8	15.9/19.9	14.9/17.3	15.4/17.5
No. atoms				
Protein	1665	1675	1708	1734
Ligand/ion	22	23	21	23
Water	296	440	566	285
B-factors (Å^2)				
Protein	12.9	11.7	6.6	10.9
Ligand/ion	8.4	6.6	3.5	7.6
Water	22.6	26.2	20.8	20.7
R.m.s. deviations				
Bond lengths (Å)	0.03	0.015	0.01	0.01
Bond angles (°)	1.42	1.39	1.36	1.41

Values for the higher resolution shell are in parentheses.

Table S2. ^{19}F NMR chemical shifts and solvent-induced isotope shifts (SIIS) of resonances (ppm) for βPGM metal fluoride TSA complexes with substrates and substrate analogs. Individual fluorine nuclei are labelled A-D in ascending order of increasing upfield chemical shift. Solvent-induced isotope shifts (ppm) for ^{19}F resonances are defined as $\delta^{19}F_{(H2O\ buffer)} - \delta^{19}F_{(100\%\ D2O\ buffer)}$.

	Complex	F_A	F_B	F_C	F_D
Step 1	βPGM-MgF_3^--βG1CF_SP	–148.4	–151.3	–180.4	–
	SIIS	1.6	1.4	0.2	–
	βPGM-MgF_3^--βG1CP	–148.1	–149.6	–181.0	–
	SIIS	1.6	1.4	0.2	–
Step 2	βPGM-MgF_3^--G6P$^{(4)}$	–147.0	–151.8	–159.0	–
	SIIS	1.6	1.4	0.9	–
	βPGM-MgF_3^--G6CP$^{(4)}$	–147.5	–153.5	–157.4	–
	SIIS	1.6	1.4	0.9	–
Step 1	βPGM-AlF_4^--βG1P	–128.5	–138.3	–141.9	–160.0
	SIIS	0.8	0.9	0.6	0.3
	βPGM-AlF_4^--βG1CF_SP	–131.7	–138.5	–139.8	–159.7
	SIIS	0.9	1.2	0.6	0.3
	βPGM-AlF_4^--βG1CP	–131.0	–138.6	–140.4	–159.8
	SIIS	0.8	1.2	0.7	0.3
Step 2	βPGM-AlF_4^--G6P$^{(5)}$	–130.6	–137.0	–140.6	–144.0
	SIIS	0.8	1.3	0.9	0.8
	βPGM-AlF_4^--G6CP	–132.2	–136.4	–141.0	–142.9
	SIIS	0.9	1.3	0.9	0.8

Table S3. Apparent dissociation constants of substrates and substrate analogs for MgF_3^- and AlF_4^- TSA complexes with βPGM, measured by titration experiments monitored by fluorescence and ^{1}H NMR.

Complex	K_d (mM)
βPGM-MgF_3^--βG1CF_SP	0.66 ± 0.07
βPGM-MgF_3^--βG1CP	1.3 ± 0.09
βPGM-MgF_3^--G6P$^{(4)}$	0.001 ± 0.0002
βPGM-MgF_3^--G6CP$^{(4)}$	0.30 ± 0.10
βPGM-AlF_4^--βG1P	0.046 ± 0.004
βPGM-AlF_4^--G6P	0.009 ± 0.001
βPGM-AlF_4^--βG1CP	1.2 ± 0.08

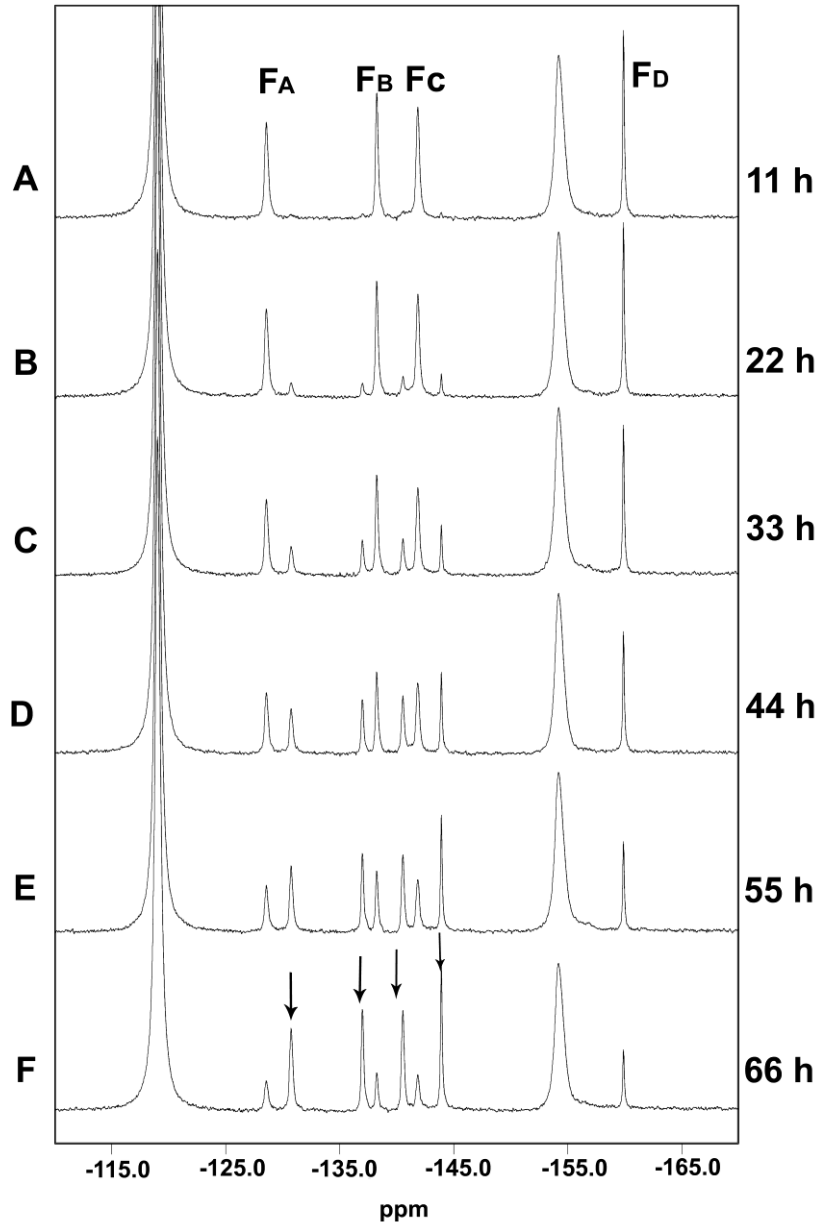

Fig. S1. ^{19}F NMR spectra recorded every 11 h show that the βPGM-AlF_4^--βG1P TSA complex (in spectrum (***A***)) readily turns into the βPGM-AlF_4^--G6P TSA complex (indicated by → in spectrum (***F***)) within 3 d. The sample is recorded for 0.5 mM βPGM, 5 mM $MgCl_2$, 1 mM $AlCl_3$, 10 mM NH_4F, 5 mM βG1P in 50 mM K^+ HEPES (pH 7.2) in 100% H_2O containing a D_2O capillary for the NMR lock.

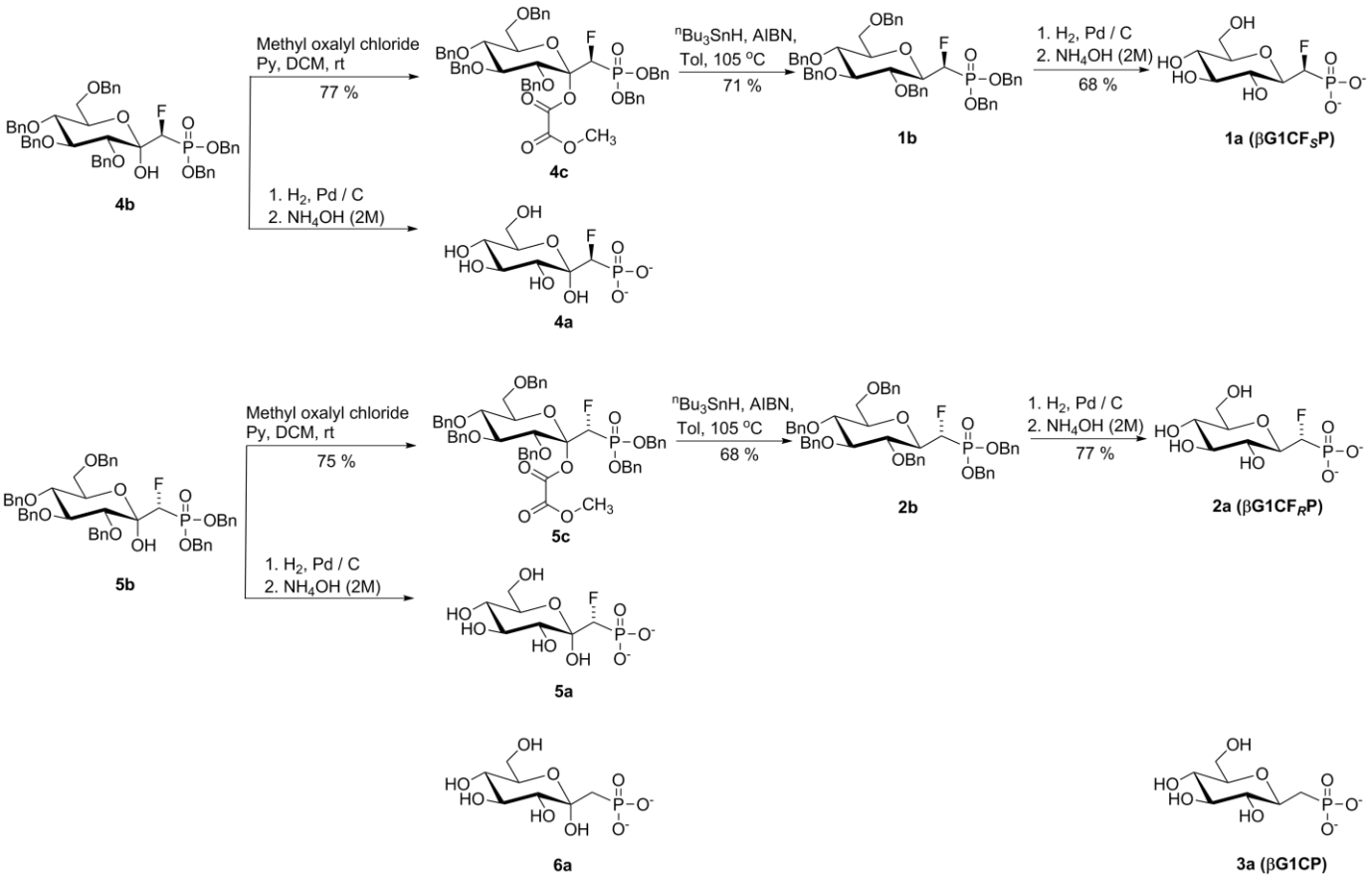

Fig. S2. Synthesis of stable analogs of βG1P, α-fluoromethylenephosphonates βG1CF$_S$P (**1a**) and βG1CF$_R$P (**2a**), as well as three 1α-hydroxy-1β-methylenephosphonates, **4a**, **5a**, and **6a**.

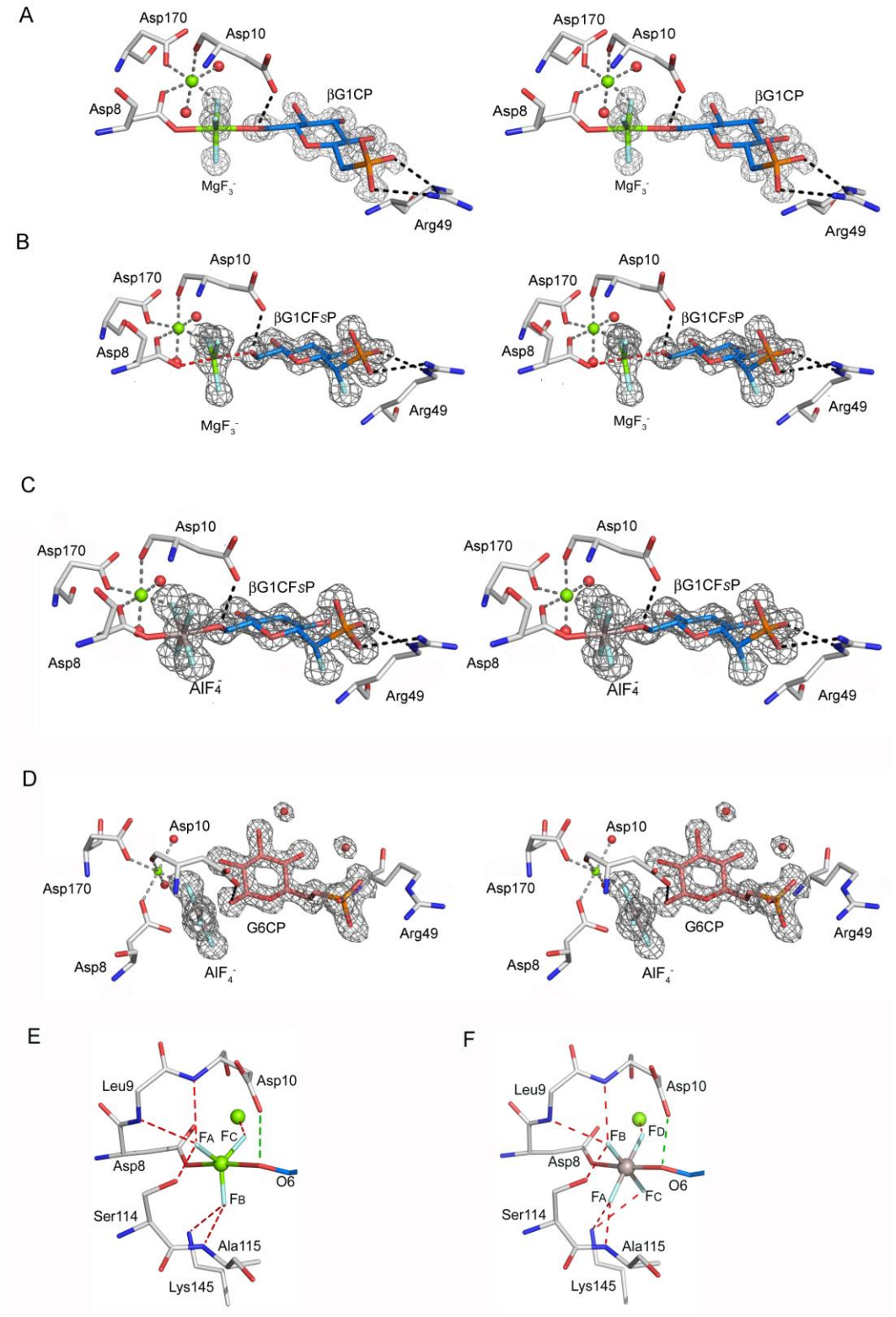

Fig. S3. Stereoview of the active sites of (*A*) the βPGM-MgF_3^--βG1CP TSA complex (**4C4R**), (*B*) the βPGM-MgF_3^--βG1CF$_S$P TSA complex (**4C4S**), (*C*) the βPGM-AlF_4^--βG1CF$_S$P TSA complex (**4C4T**), and (*D*) the βPGM-AlF_4^--G6CP TSA complex (**2WF7**; **Table S1**). Difference density ($F_o - F_c$) for MgF_3^-, AlF_4^-, βG1CP, βG1CF$_S$P, G6CP and two conserved waters are shown as gray mesh contoured at 4σ. (*E*) The ^{19}F assignments for the MgF_3^- moiety in the crystal structures of TSA complexes for Step 1. (*F*) The ^{19}F assignments for the AlF_4^- moiety in the crystal structure of TSA complexes for Step 1. The hydrogen bond coordination for the metal fluorides are shown as red dashed lines (the hydrogen bond with the general base is colored in green), with magnesium in green, aluminum in gray and fluorines as pale blue sticks.

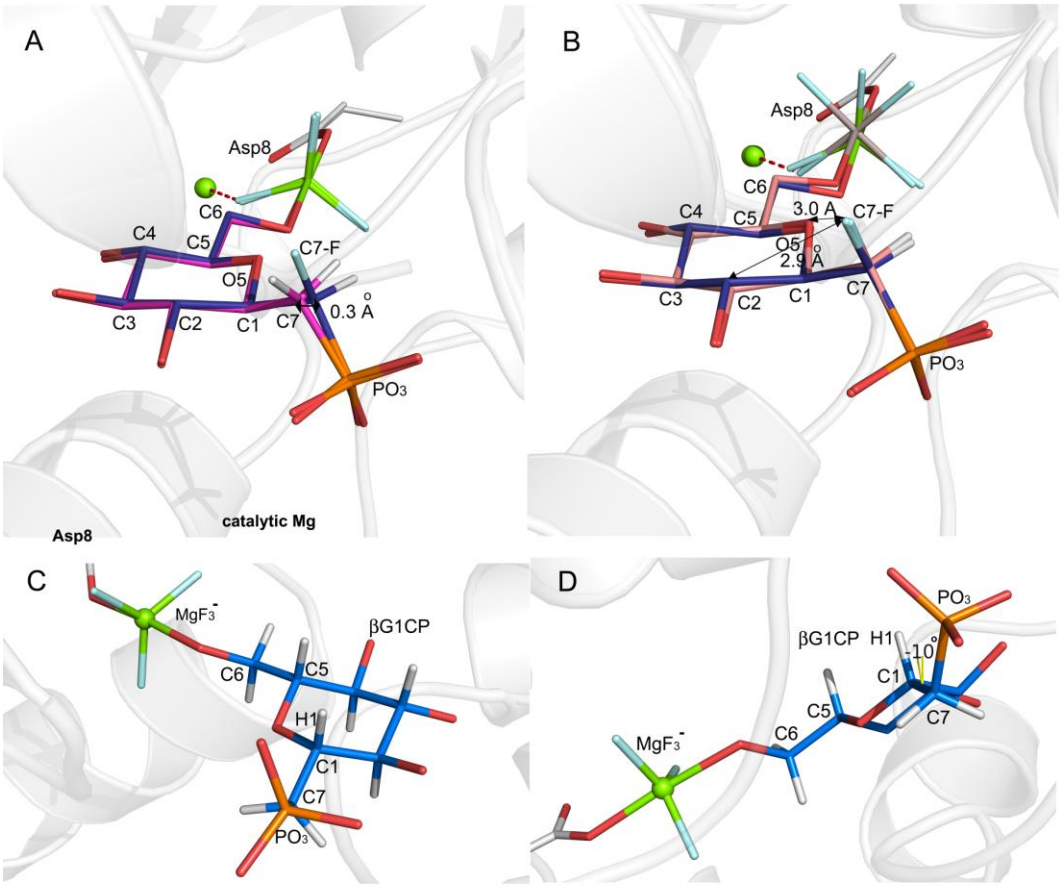

Fig. S4. Comparison of the metal fluoride TSA complexes of βG1CF$_S$P and βG1CP shows the steric effect of C7-fluorine substitution. (*A*) The C7 atom in the βPGM-MgF_3^--βG1CF$_S$P (purple) and the C7 atom in the βPGM-MgF_3^--βG1CP (magenta) TSA complexes have a positional separation of 0.3 Å due to C7-fluorine substitution. (*B*) The C1–C7 bond in βG1CF$_S$P in the βPGM-MgF_3^--βG1CF$_S$P (purple) and the βPGM-AlF_4^--βG1CF$_S$P (pink) TSA complexes has rotated to reduce the eclipsed interaction between the C7-fluorine and C2 (2.9 Å), while maintaining a separation of 3.0 Å between the C7-fluorine and O5. The magnesiums are in green (catalytic, sphere; surrogate, sticks), aluminum in gray, fluorines as pale blue sticks, hydrogens as white sticks, and protein as gray cartoon. (*C*) The C7 methylene is in a staggered conformation with the 1-phosphonate oxygen atoms. (*D*) The P–C7 bond eclipses H1 on the glucopyranose ring with a dihedral angle of –10 °. The surrogate magnesium is shown as a green sphere, with fluorines as pale blue sticks, βG1CP as blue sticks with hydrogen atoms in white, and protein as a gray cartoon.

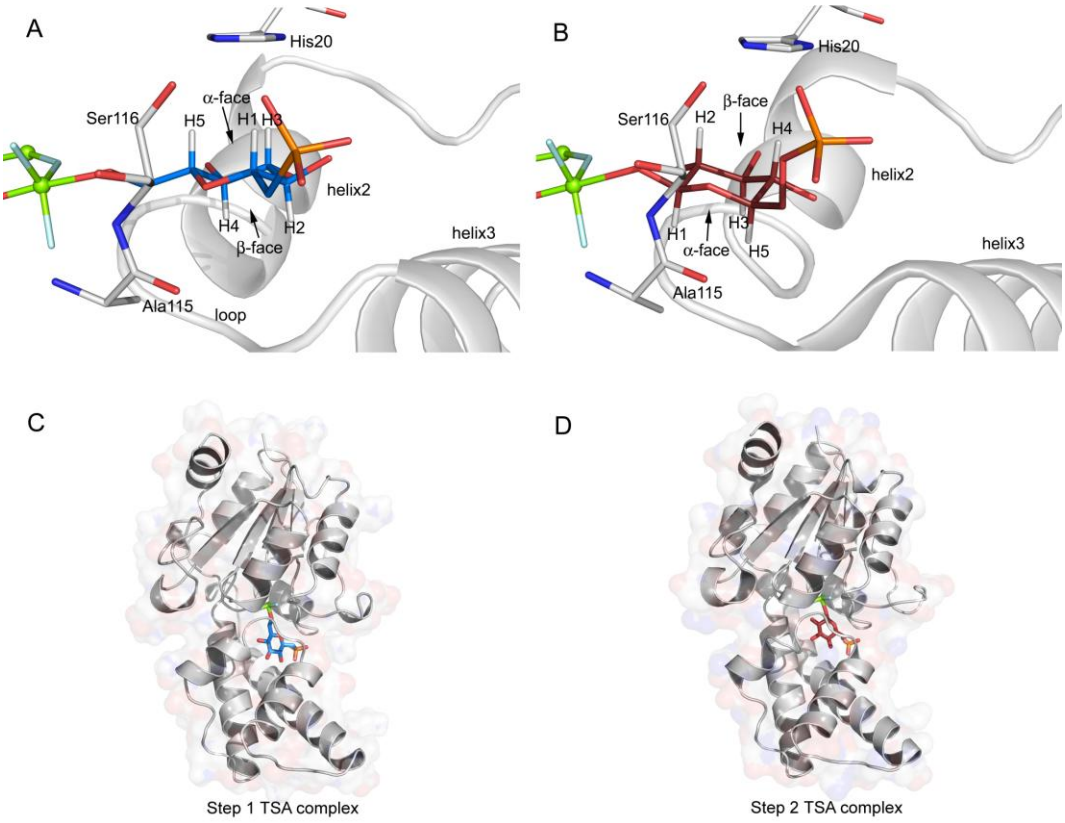

Fig. S5. The comparison of glucopyranose orientation in the βPGM-MgF_3^- TSA complexes of βG1CP (step 1) and G6P (step 2). (*A*) His20 caps the α-face of the glucopyranose ring of βG1CP (blue) in the βPGM-MgF_3^--βG1CP TSA complex. The loop between helices 2 and 3 (in gray cartoon) caps the β-face of the ring. (*B*) His20 caps the β-face of the glucopyranose ring of G6P (ruby) in the βPGM-MgF_3^--G6P TSA complex. The inert phosphate moiety has a conformation *anti* to H5. The loop between helices 2 and 3 (in gray cartoon) caps the α-face of the ring. In both complexes, Ala115 and Ser116 (shown as sticks) flank the substrate cavity on one side. (*C*) The overall closed structure of the βPGM-MgF_3^--βG1CP TSA complex (Step 1) with the substrate βG1CP in blue sticks and the protein as a gray cartoon. (*D*) The overall closed structure of the βPGM-MgF_3^--G6P TSA complex (Step 2) with the substrate G6P in red sticks and the protein as a gray cartoon. The backbone atoms of the βPGM-MgF_3^--βG1CP TSA complex overlay with those of the βPGM-MgF_3^--G6P TSA complex with rmsd 0.202 Å.

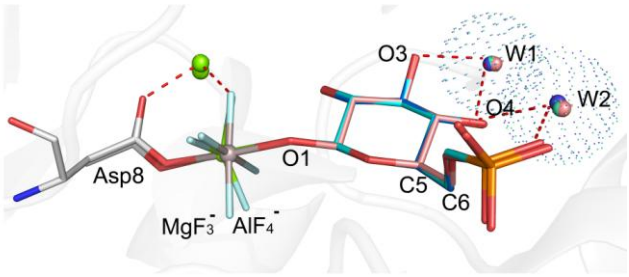

Fig. S6. Superposition of TSA complexes for βPGM-MgF_3^--G6P (blue, PDB 2WF5), βPGM-AlF_4^--G6P (pink, PDB 2WF6) and βPGM-AlF_4^--G6CP (cyan, PDB 2WF7). G6CP is the G6P analog, 6-phosphonomethylene-6-deoxyglucopyranose. In all three βPGM TSA complexes, W1 and W2 are two conserved waters (highlighted by blue dotted spheres). W1 always coordinates 3-OH and 4-OH, while W2 coordinates 4-OH and the 6-phosphate in G6P (6-phosphonate in G6CP). The magnesiums are shown in green, with aluminum in gray, and fluorines as pale blue sticks.

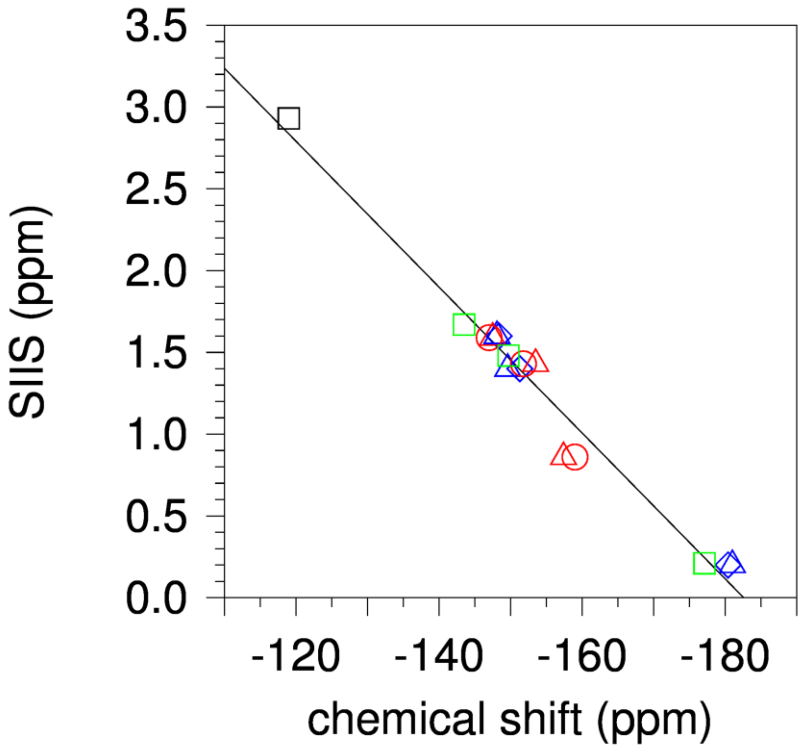

Fig. S7. Correlation plot showing the relationship between chemical shift (ppm) and SIIS ($\delta_{H2O} - \delta_{D2O}$, ppm) for the ^{19}F resonance of free F^- (black square) and those of the following βPGM-MgF_3^- TSA complexes: βPGM-MgF_3^--βG1CF_SP (blue diamonds), βPGM-MgF_3^--βG1CP (blue triangles), βPGM-MgF_3^--G6P (red circles), βPGM-MgF_3^--G6CP (red triangles) and βPGM-MgF_3^--2deoxyG6P (4) (green squares). Linear regression analysis gives $R^2 = 0.97$.

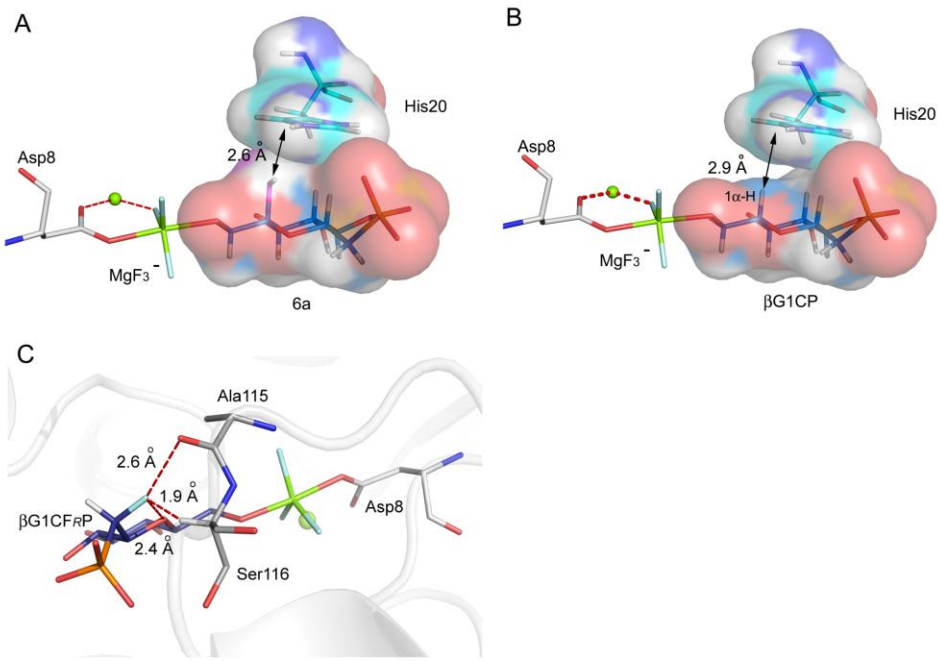

Fig. S8. (*A*) Modeling of a 1α-OH group onto βG1CP in the crystal structure of the βPGM-MgF_3^--βG1CP TSA complex to mimic the binding of **6a** (in blue sticks) shows the steric opposition with His20 due to an unacceptable van der Waals clash (2.6 Å) of the 1α-OH oxygen of **6a** with Cδ2 of the His20 imidazole ring. (*B*) The unmodified βPGM-MgF_3^--βG1CP TSA complex shows there is no van der Waals clash (2.9 Å) of the 1α-H of βG1CP with the His20 imidazole ring. (*C*) Modeled binding confirmation of the (*R*)-isomer, βG1CF_RP, in the βPGM-MgF_3^--βG1CF_RP TSA complex based on the βPGM-MgF_3^--βG1CP TSA complex (**4C4R**) to show the steric clashes for the C7-fluorine in the active site. The distances from the C7-fluorine to nearby atoms are too short to avoid steric clashes: 2.6 Å to the backbone carbonyl oxygen of Ala115, 1.9 Å to the Hα of Ser116, and 2.4 Å to the glucopyranose ring oxygen (van der Waals radii are: oxygen 1.57 Å, fluorine 1.47 Å, and hydrogen 1.20 Å). Distances are shown as red dashes, with βG1CF_RP in purple, magnesium in green, fluorines in pale blue, hydrogens in white, and the protein in gray.

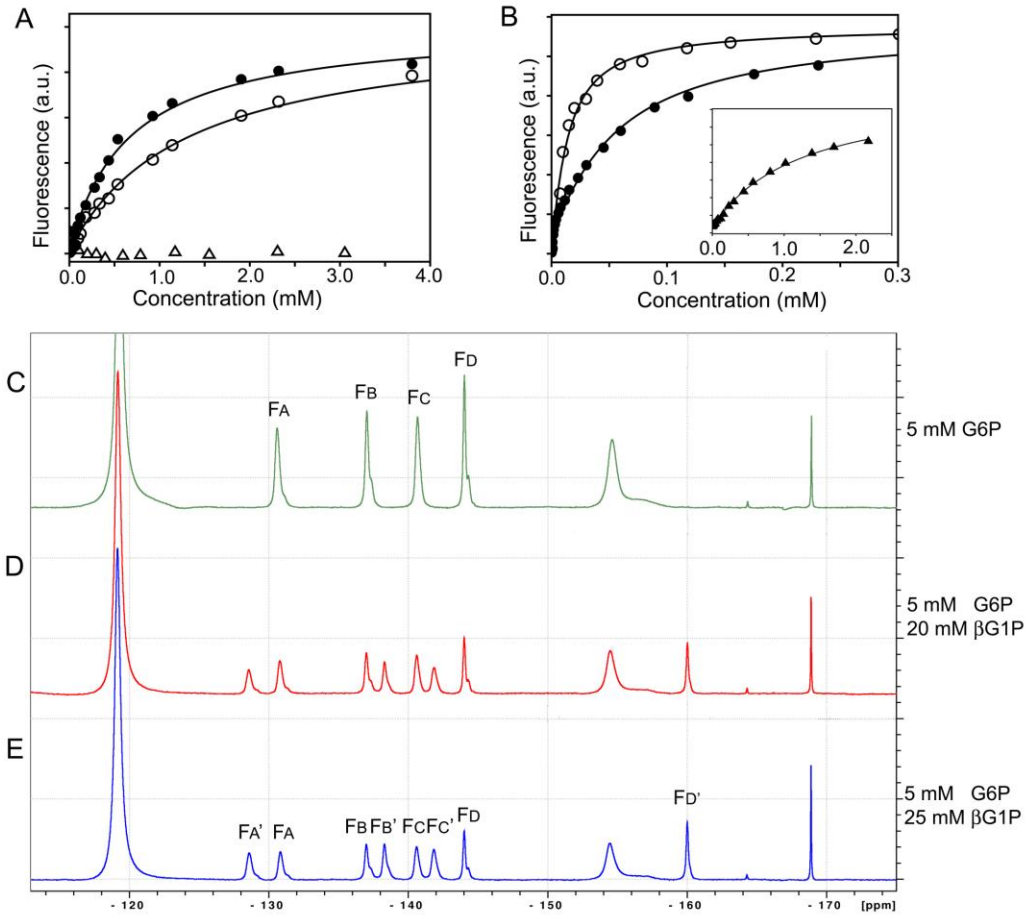

Fig. S9. Determination of the apparent dissociation constants K_d of step 1 and step 2 substrates in their metal fluoride TSA complexes. (*A*) Fluorescence titrations to measure the apparent dissociation constants K_d for βG1CF$_S$P (●), βG1CF$_R$P (Δ) and βG1CP (○) for the βPGM-MgF_3^- TSA complexes. (*B*) Fluorescence titrations to measure the apparent dissociation constants K_d for βG1P (●), G6P (○), and βG1CP (▲, inset) for the βPGM-AlF_4^- TSA complexes. (*C-E*) Determination of the relative dissociation constants of βG1P and G6P in their AlF_4^- TSA complexes. (*C*) ^{19}F NMR spectrum of the βPGM-AlF_4^--G6P TSA complex with 5 mM G6P in the sample. The four fluorines in the AlF_4^- moiety are assigned according to their chemical shifts (4). (*D*) 20 mM βG1P was added to (*C*) resulting in a mixture of the βPGM-AlF_4^--G6P TSA and βPGM-AlF_4^--βG1P TSA complexes. (*E*) A further 5 mM βG1P was added to (*D*) resulting in a 1:1 ratio of the βPGM-AlF_4^--G6P TSA and βPGM-AlF_4^--βG1P TSA complexes according to peak integration. The four fluorines in βPGM-AlF_4^--βG1P TSA complex are denoted by a '' symbol. All the samples contained 1.0 mM βPGM, 5 mM $MgCl_2$, 2 mM $AlCl_3$, 20 mM NH_4F and 10% D_2O in 50 mM K^+ HEPES (pH 7.2). All three experiments were completed within 30 min to minimize any effects due to residual mutase activity of the enzyme (**Fig. S1**).

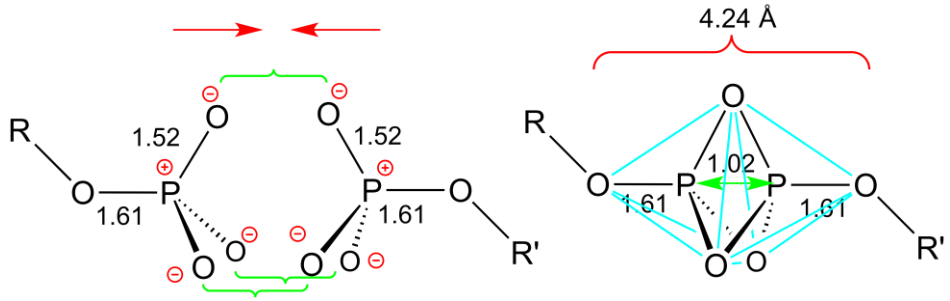

Fig. S10. Geometry for phosphoryl group transfer. Full convergence of non-bridging oxygens for two phosphate monoesters (left, red arrows) generates a tbp complex (right) (tbp edges in cyan). Phosphoryl transfer requires translocation of phosphorus atom 1.02 Å across the medial plane (geometry using standard bond lengths and angles) (51).

A

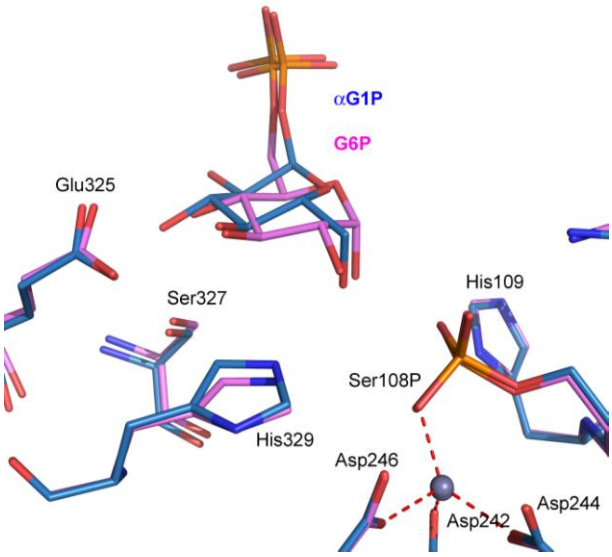

B

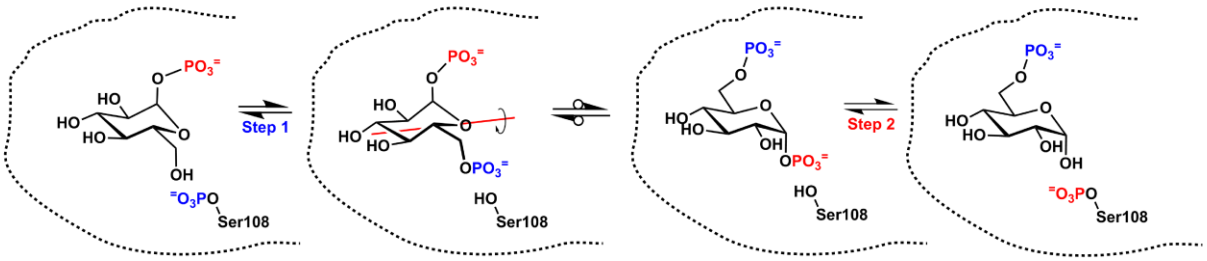

Fig. S11. The active site of αPMM/PGM for step 1 and step 2 complexes in the near-attack confirmation. (*A*) Overlay (based on all protein Cα) of the substrates αG1P (cpk-mid blue, PDB **1P5D**) and G6P (cpk-magenta, PDB **1P5G**) in Ser108-phosphorylated αPMM/PGM, illustrating the constant conformation of the C5-C6 exocyclic bond for Step 1 and Step 2. Direct recognition for 3-OH and 4-OH is achieved by Glu325 and Ser327. Zinc atoms are shown as purple spheres and phosphorus atoms are in orange. (*B*) Scheme to show how interchange of the 1α-phosphate and the 6-phosphate between Step 1 and Step 2 in αPMM/PGM can be accomplished simply by rotation of the hexose bisphosphate about a virtual 2-fold C2 axis defined by the ring oxygen and the midpoint of the C3–C4 bond. The conformation of the exocyclic C5–C6 bond remains the same.

General methods for synthesis.

All reagents and anhydrous solvents were purchased and used without further purification. Non-aqueous reactions were performed under a N_2 atmosphere unless otherwise indicated. Reaction progress was monitored by thin-layer chromatography on silica gel 60 F_{254} silica plates (Silicycle). TLC plates were visualized by dipping in a solution of *p*-anisaldehyde (3.4%), sulfuric acid (2.2%), and acetic acid (1.1%) in ethanol, followed by charring. NMR spectra were recorded on Bruker AV-300 or AV-500 NMR spectrometers at the Nuclear Magnetic Resonance Research Resource (NMR-3), Dalhousie University. Low resolution mass spectra were obtained using an Applied Biosystems hybrid triple quadrupole linear ion trap (Q2000trap) mass spectrometer equipped with an electrospray ionization (ESI) source. For sample analysis, the mass spectrometer was coupled to an Agilent 1100 HPLC instrument fitted with a Phenomenex Kinetex 2.6u (150 × 2.10 mm) column. Samples were run using an isocratic method with 70/30 CH_3CN / 2 mM aqueous ammonium acetate (pH 5.5) at a flow rate of 120 µL·min^{-1}. The capillary voltage was set to ±4500 kV with a declustering potential of ±60 V and the curtain gas was set to 20 (arbitrary units) for positive and negative mode, respectively. Analysis software used was Analyst version 1.4.1 (Applied Biosystems).

Synthesis of 2,3,4,6-tetra-*O*-benzyl-1-deoxy-1-methyloxoacetato-*C*-(1'*R*-fluoro-dibenzylphosphonomethyl)-β-D-glucopyranoside (5c) and 2,3,4,6-tetra-*O*-benzyl-1-deoxy-1-methyloxoacetato-*C*-(1'*S*- fluoro-dibenzylphosphonomethyl)-β-D-glucopyranoside (4c) (21).

Methyl chlorooxoacetate (0.45 mL, 4.92 mmol) was added dropwise to a solution of the *C*-1′R fluoroketose phosphonate derivative **5b** (18) (410 mg, 0.49 mmol) in anhydrous CH_2Cl_2 (7 mL) containing pyridine (2 mL) with vigorous stirring at rt. After 1 h, EtOH (1.5 mL) was added and the mixture was stirred at rt for 10 min. The reaction mixture was diluted with EtOAc (15 mL) and washed successively with saturated aqueous $NaHCO_3$ (20 mL), water (15 mL) and brine (5 mL). The organic phase was dried over anhydrous Na_2SO_4 and concentrated under reduced pressure. The crude product was purified by silica gel flash column chromatography with ethyl acetate/hexanes (3:7) to give compound **5c** (339 mg, 75%) as a thick colorless oil. TLC (hexanes:EtOAc, 75:25 v/v): R_f = 0.30; ^{1}H NMR (500 MHz, $CDCl_3$): δ 7.34-7.23 (m, 28H, aromatic CH), 7.18-7.16 (m, 2H, aromatic CH), 6.26 (dd, *J* = 44.5, 6.5 Hz, 1H, H-1′), 5.21-5.11 (m, 2H, CH_2Ph), 5.09-5.07 (m, 2H, CH_2Ph), 4.89-4.81 (m, 5H, 2xCH_2Ph, CHPh), 4.60 (d, *J* = 11.0 Hz, 1H, CHPh), 4.43 (d, *J* = 11.5 Hz, 1H, CHPh), 4.32(d, *J* = 11.5 Hz, 1H, CHPh), 4.26-4.24 (m, 1H, H-5), 4.18 (dd, *J* = 9.5, 2.9 Hz, 1H, H-2), 4.05 (t, *J* = 9.5 Hz, 1H, H-3), 3.88 (s, 3H, O-CH_3), 3.85 (t, *J* = 9.7 Hz, 1H, H-4), 3.83 (dd, *J* = 11.2, 3.4 Hz, 1H, H-6a), 3.72 (dd, *J* = 11.2, 1.5 Hz, 1H, H-6b); ^{13}C NMR (125 MHz, $CDCl_3$): δ 157.5 (C=O), 154.1 (C=O), 138.2, 137.7 (2C), 137.4 (4x quaternary aromatic C), 136.1 (d, *J* = 6.7 Hz), 135.8 (d, *J* = 6.7 Hz) (2x quaternary aromatic C), 128.5, 128.4, 128.3, 128.0 (2C), 127.9, 127.8, 127.7, 127.6 (aromatic CH), 106.3 (d, $^2J_{C\text{-}P}$ = 20.7 Hz, C-1), 85.1 (dd, $^1J_{C\text{-}F\ and\ C\text{-}P}$ = 192.2, 164.9 Hz, C-1′), 82.6 (C-3), 78.9 (d, $^3J_{C\text{-}P}$ = 5.0 Hz, C-2), 76.6 (CH_2Ph), 75.8 (C-4), 75.5 (CH_2Ph), 75.3 (CH_2Ph), 74.3 (C-5), 73.3 (CH_2Ph), 68.7 (d, $^2J_{C\text{-}P}$ = 5.8 Hz, P(O)O-CH_2Ph), 68.2 (d, $^2J_{C\text{-}P}$ = 5.8 Hz, P(O)O-CH_2Ph), 68.0 (C-6), 53.7 (O-CH_3); ^{31}P{^{1}H} NMR (202.5 MHz, $CDCl_3$): δ 13.3 (d, $^2J_{P\text{-}F}$ = 70.3 Hz, 1P); ^{19}F{^{1}H} NMR (282.4 MHz, $CDCl_3$): δ −210.69 (d, $^2J_{F\text{-}P}$ = 70.3 Hz, 1F); ^{19}F NMR (282.4 MHz, $CDCl_3$): δ −210.69 (dd, $^2J_{F\text{-}P\ and\ F\text{-}H}$ = 70.3, 45.4 Hz, 1F); LRMS (ESI, positive mode)(m/z): $[M+H_2O]^+$ calcd for $C_{52}H_{52}FO_{12}P$, 936.3; found, 936.1.

The same reaction conditions with the *C*-1′*S*-fluoroketose phosphonate derivative **4b** (272 mg, 0.33 mmol) produced the *S*-oxalate ester **4c** as a colorless oil (231 mg, 77%). TLC (hexanes:EtOAc, 75:25 v/v): R_f = 0.50; ^{1}H NMR (500 MHz, $CDCl_3$): δ 7.36-7.27 (m, 26H, aromatic CH), 7.22-7.20 (m, 2H, aromatic CH), 7.18-7.16 (m, 2H, aromatic CH), 6.10 (dd, *J* = 42.4, 6.9 Hz, 1H, H-1′), 5.27-5.18 (m, 2H, CH_2Ph), 5.00-4.95 (m, 2H, CH_2Ph), 4.91-4.84 (m, 5H, 2x CH_2Ph, CHPh), 4.71 (d, *J* = 9.0 Hz, 1H, H-2), 4.63 (d, *J* = 10.5 Hz, 1H, CHPh), 4.31 (m, 2H, CH_2Ph), 4.25-4.23 (m, 1H, H-5), 4.06-4.05 (m, 2H, H-3 and H-4), 3.94 (s, 3H, O-CH_3), 3.87 (dd, *J* = 11.0, 3.2 Hz, 1H, H-6a), 3.78 (dd, *J* = 11.2, 2.1 Hz, 1H, H-6b); ^{13}C NMR (125 MHz, $CDCl_3$): δ 157.8 (C=O), 153.2 (C=O), 138.3, 137.8, 137.6, 137.4 (4x quaternary aromatic C), 136.2 (d, *J* = 6.0 Hz), 135.4 (d, *J* = 6.0) (2x quaternary aromatic C), 128.5, 128.4, 128.3, 128.1, 128.0, 127.8 (2C), 127.7, 127.6, 127.5 (2C), 127.3 (aromatic CH), 107.5 (dd, $^2J_{\text{C-F and C-P}}$ = 16.0, 7.8 Hz, C-1), 86.2 (dd, $^1J_{\text{C-F and C-P}}$ = 199.9, 162.9 Hz, C-1′), 82.9 (C-4), 79.8 (C-2), 76.5 (C-3), 75.5 (CH_2Ph), 75.4 (CH_2Ph), 75.3 (C-5), 74.3 (CH_2Ph), 73.1 (CH_2Ph), 69.7 (d, $^2J_{\text{C-P}}$ = 5.9 Hz, P(O)OCH_2Ph), 68.1 (d, $^2J_{\text{C-P}}$ = 6.7 Hz, P(O)OCH_2Ph), 67.8 (C-6), 53.7 (O-CH_3); ^{31}P{^{1}H} NMR (202.5 MHz, $CDCl_3$): δ 12.3 (d, $^2J_{\text{P-F}}$ = 66.2 Hz, 1P); ^{19}F{^{1}H} NMR (282.4 MHz, $CDCl_3$): δ −217.09 (d, $^2J_{\text{F-P}}$ = 66.2 Hz, 1F); ^{19}F NMR (282.4 MHz, $CDCl_3$): δ −217.09 (dd, $^2J_{\text{F-P and F-H}}$ = 66.2, 42.4 Hz, 1F); HRMS (ESI, positive mode)(m/z): $[M+Na]^+$ calcd for $C_{52}H_{52}FO_{12}P$, 941.3073; found, 941.3071.

Synthesis of 2,3,4,6-tetra-*O*-benzyl-1-deoxy-*C*-(1'*R*-fluoro-dibenzylphosphonomethyl)-β-D-glucopyranoside (2b) and 2,3,4,6-tetra-*O*-benzyl-1-deoxy-*C*-(1'*S*-fluoro-dibenzylphosphonomethyl)-β-D-glucopyranoside (1b) (20,22**).**

A solution of the *C*-1′*R*-fluoro configured oxalate ester **5c** (250 mg, 0.27 mmol), *n*-Bu_3SnH (0.15 mL, 0.54 mmol) and AIBN (0.27 mL, 0.05 mmol, 0.2 M in toluene) in dry and degassed toluene (10 mL) was refluxed for 30 min. The solution was cooled, and water added. The organic phase was extracted with ethyl acetate (3x10 mL) and dried with anh. Na_2SO_4. The combined organic phase was evaporated under reduced pressure and the crude product obtained was chromatographed on silica gel with ethyl acetate/hexane (3:7) as the eluent to afford the deoxygenated compound **2b** (151 mg, 68%) as a thick colorless oil. TLC (hexanes:EtOAc, 75:25 v/v): R_f = 0.30; ^{1}H NMR (500 MHz, $CDCl_3$): δ 7.34-7.27 (m, 28H, aromatic CH), 7.20-7.18 (m, 2H, aromatic CH), 5.24-5.22 (m, 2H, CH_2Ph), 5.13 (dd, *J* = 43.4, 8.8 Hz, 1H, H-1′), 5.07-5.03 (m, 2H, CH_2Ph), 4.97-4.93 (m, 3H, CH_2Ph, CHPh), 4.86 (d, *J* = 10.8 Hz, 1H, CHPh), 4.67 (d, *J* = 11.5 Hz, 1H, CHPh), 4.60 (d, *J* = 11.5 Hz, 1H, CHPh), 4.44 (d, *J* = 11.5 Hz, 1H, CHPh), 4.36 (d, *J* = 11.5 Hz, 1H, CHPh), 3.89-3.78 (m, 3H, H-1, H-2 and H-4), 3.71 (m, 2H, H-6a and H-6b), 3.67 (t, *J* = 9.4 Hz, 1H, H-3), 3.63-3.61 (m, 1H, H-5); ^{13}C NMR (125 MHz, $CDCl_3$): δ 138.3, 137.8 (2C), 137.7, 136.4 (d, *J* = 6.2 Hz), 135.8 (d, *J* = 6.2 Hz) (6x quaternary aromatic C), 128.5, 128.4 (2C), 128.3, 128.0, 127.9, 127.8 (2C), 127.7 (2C), 127.5 (aromatic CH), 86.9 (C-2), 86.4 (dd, $^1J_{\text{C-F and C-P}}$ = 192.2, 170.1 Hz, C-1′), 79.4 (C-5), 77.9 (C-3), 77.4 (C-1), 76.6 (C-4), 75.6 (CH_2Ph), 75.1 (2x CH_2Ph), 73.2 (CH_2Ph), 69.0 (d, $^2J_{\text{C-P}}$ = 6.7 Hz, P(O)O-CH_2Ph), 68.9 (C-6), 67.8 (d, $^2J_{\text{C-P}}$ = 6.7 Hz, P(O)O-CH_2Ph); ^{31}P{^{1}H} NMR (121.5 MHz, $CDCl_3$): δ 16.7 (d, $^2J_{\text{P-F}}$ = 72.7 Hz, 1P); ^{19}F{^{1}H} NMR (282.4 MHz, $CDCl_3$): δ −222.43 (d, $^2J_{\text{F-P}}$ = 72.7 Hz, 1F); ^{19}F NMR (282.4 MHz, $CDCl_3$): δ −222.43 (ddd, $^2J_{\text{F-P}}$ = 72.7 Hz, $^2J_{\text{F-H-1′}}$ = 43.4 Hz, $^3J_{\text{F-H-1}}$ = 29.6 Hz, 1F); LRMS (ESI, positive mode)(m/z): $[M+H_2O]^+$ calcd for $C_{49}H_{50}FO_8P$, 834.3; found, 834.1.

The same reaction conditions with the *C*-1′*S*-fluoro configured oxalate ester **4c** (141 mg, 0.15 mmol) produced the corresponding deoxygenated derivative **1b** as a colorless oil (89 mg, 71%). TLC (Hexanes:EtOAc, 75:25 v/v): R_f =

0.50; ^{1}H NMR (500 MHz, $CDCl_3$): δ 7.37-7.26 (m, 26H, aromatic CH), 7.21-7.19 (m, 2H, aromatic CH), 7.18-7.16 (m, 2H, aromatic CH), 5.31-5.27 (m, 1H, CHPh), 5.22-5.20 (m, 1H, CHPh), 5.19 (ddd, *J* = 43.4, 7.8, 2.0 Hz, 1H, H-1′), 5.09-4.95 (m, 5H, 2x CH_2Ph, CHPh), 4.86 (d, *J* = 10.7 HZ, 1H, CHPh), 4.78 (d, *J* = 10.7 HZ, 1H, CHPh), 4.61 (d, *J* = 10.7 HZ, 1H, CHPh), 4.31 (m, 2H, CH_2Ph), 4.24 (t, *J* = 9.6 Hz, 1H, H-2), 4.02-3.94 (m, 1H, H-1), 3.90 (t, *J* = 9.5 Hz, 1H, H-4), 3.80-3.72 (m, 3H, H-6a, H-6b and H-3), 3.54-3.51 (m, 1H, H-5); ^{13}C NMR (125 MHz, $CDCl_3$): δ 138.5, 138.0 (2C), 137.7 (4x quaternary aromatic C), 136.7 (d, *J* = 6.3 Hz), 135.9 (d, *J* = 6.3 Hz) (2x quaternary aromatic C), 128.5, 128.4, 128.3, 128.1, 128.0 127.9 (2C), 127.8 (2C), 127.6, 127.5, 127.3, 87.7 (dd, $^{1}J_{\text{C-F and C-P}}$ = 189.2, 166.2 Hz, C-1′), 87.4 (C-3), 80.1 (d, $^{2}J_{\text{C-F}}$ = 19.5 Hz, C-1), 79.1 (C-5), 77.9 (C-2), 77.6 (C-4), 75.3 (CH_2Ph), 75.1 (CH_2Ph), 75.0 (CH_2Ph), 73.1 (CH_2Ph), 69.1 (d, $^{2}J_{\text{C-P}}$ = 5.4 Hz, P(O)OCH_2Ph), 68.6 (C-6), 67.5 (d, $^{2}J_{\text{C-P}}$ = 6.7 Hz, P(O)OCH_2Ph); ^{31}P{^{1}H} NMR (202.5 MHz, $CDCl_3$): δ 15.6 (d, $^{2}J_{\text{P-F}}$ = 70.9 Hz, 1P); ^{19}F{^{1}H} NMR (282.4 MHz, $CDCl_3$): δ −209.13 (d, $^{2}J_{\text{F-P}}$ = 70.9 Hz, 1F); ^{19}F NMR (282.4 MHz, $CDCl_3$): δ −209.13 (ddd, $^{2}J_{\text{F-P}}$ = 70.9 Hz, $^{2}J_{\text{F-H-1′}}$ = 43.4 Hz, $^{3}J_{\text{F-H-1}}$ = 20.8 Hz, 1F); HRMS (ESI, positive mode)(m/z): $[M+Na]^+$ calcd for $C_{49}H_{50}FO_8P$, 839.3120; found, 839.3125.

Synthesis of ammonium 1-deoxy-*C*-(1'*R*-fluoro-phosphonomethyl)-β-D-glucopyranoside (2a) (βG1CF$_R$P) and ammonium 1-deoxy-*C*-(1'*S*-fluoro-phosphonomethyl)-β-D-glucopyranoside (1a) (βG1CF$_S$P).

A vigorously stirred mixture of the deoxygenated fluorosugar **2b** (120 mg, 0.15 mmol), 10% palladium on carbon (32 mg, 20 mol%), ethyl acetate (5 mL) and methanol (5 mL) was degassed under vacuum and saturated with hydrogen under 1 atm. pressure. The suspension was stirred at room temperature 6 h, then filtered through (Celite) and concentrated to give the free phosphonic acid derivative as a colorless oil. The oil was taken up in water (1.5 mL) and immediately adjusted to *p*H 8 with NH_4OH (2 M), concentrated and lyophilized to give the target phosphonate **2a** (35 mg, 77%) as a colourless foam. ^{1}H NMR (500 MHz, D_2O): δ 4.67 (ddd, *J* = 42.3, 8.3, 3.9 Hz, 1H, H-1′), 3.88 (dd, *J* = 12.6, 1.5 Hz, 1H, H-6a), 3.68-3.59 (m, 2H, H-6b and H-1), 3.51-3.45 (m, 2H, H-4 and H-3), 3.40-3.36 (m, 1H, H-5), 3.34-3.31 (m, 1H, H-2); ^{13}C NMR (125 MHz, D_2O): δ 90.3 (dd, $^{1}J_{\text{C-F and C-P}}$ = 179.1, 149.8 Hz, C-1′), 79.6 (C-5), 78.8 (d, *J* = 17.1 Hz, C-1), 77.2 (C-3), 69.6 (C-2), 69.3 (C-4), 60.7 (C-6); ^{31}P{^{1}H} NMR (202.5 MHz, D_2O): δ 9.1 (d, $^{2}J_{\text{P-F}}$ = 64.5 Hz, 1P); ^{19}F{^{1}H} NMR (282.4 MHz, D_2O): δ −216.17 (d, $^{2}J_{\text{F-P}}$ = 64.5 Hz, 1F); ^{19}F NMR (282.4 MHz, D_2O): δ −216.17 (ddd, $^{2}J_{\text{F-P}}$ = 64.5 Hz, $^{2}J_{\text{F-H-1′}}$ = 42.3 Hz, $^{3}J_{\text{F-H-1}}$ = 24.7 Hz, 1F); HRMS (ESI, negative mode)(m/z): $[M-H]^-$ calcd. for $C_7H_{14}FO_8P$, 275.0338; found, 275.0338.

The same reaction conditions with the *C*-1′*S*-configured deoxygenated fluorosugar **1b** (72 mg, 0.09 mmol) produced the *C*-1′*S*-configured target phosphonate **1a** as a colorless foam (23 mg, 84%). ^{1}H NMR (500 MHz, D_2O): δ 4.78 (dd, *J* = 39.5, 10.2 Hz, 1H, H-1′), 3.88 (dd, *J* = 12.5, 2.3 Hz, 1H, H-6a), 3.77 (t, *J* = 9.6 Hz, 1H, H-1), 3.73-3.70 (m, 1H, H-2), 3.64 (dd, *J* = 12.3, 6.6 Hz, 1H, H-6b), 3.51 (t, *J* = 9.5 Hz, 1H, H-3), 3.46-3.43 (m, 1H, H-5), 3.30 (t, *J* = 9.5 Hz, 1H, H-4); ^{13}C NMR (125 MHz, D_2O): δ 93.5 (dd, $^{1}J_{\text{C-F and C-P}}$ = 178.8, 150.6 Hz, C-1′), 79.6 (C-2), 78.9 (C-5), 77.4 (C-3), 69.5 (C-1), 68.2 (C-4), 61.1 (C-6); ^{31}P{^{1}H} NMR (202.5 MHz, D_2O): δ 8.7 (d, $^{2}J_{\text{P-F}}$ = 60.7 Hz, 1P); ^{19}F{^{1}H} NMR (282.4 MHz, D_2O): δ −217.24 (d, $^{2}J_{\text{F-P}}$ = 60.7 Hz, 1F); ^{19}F NMR (282.4 MHz, D_2O): δ −217.24 (ddd, $^{2}J_{\text{F-P}}$ = 60.7 Hz, $^{2}J_{\text{F-H-1′}}$ = 39.5 Hz, $^{3}J_{\text{F-H-1}}$ = 29.7 Hz, 1F); HRMS (ESI, negative mode)(m/z): $[M-H]^-$ calcd. for $C_7H_{14}FO_8P$, 275.0338; found, 275.0331.

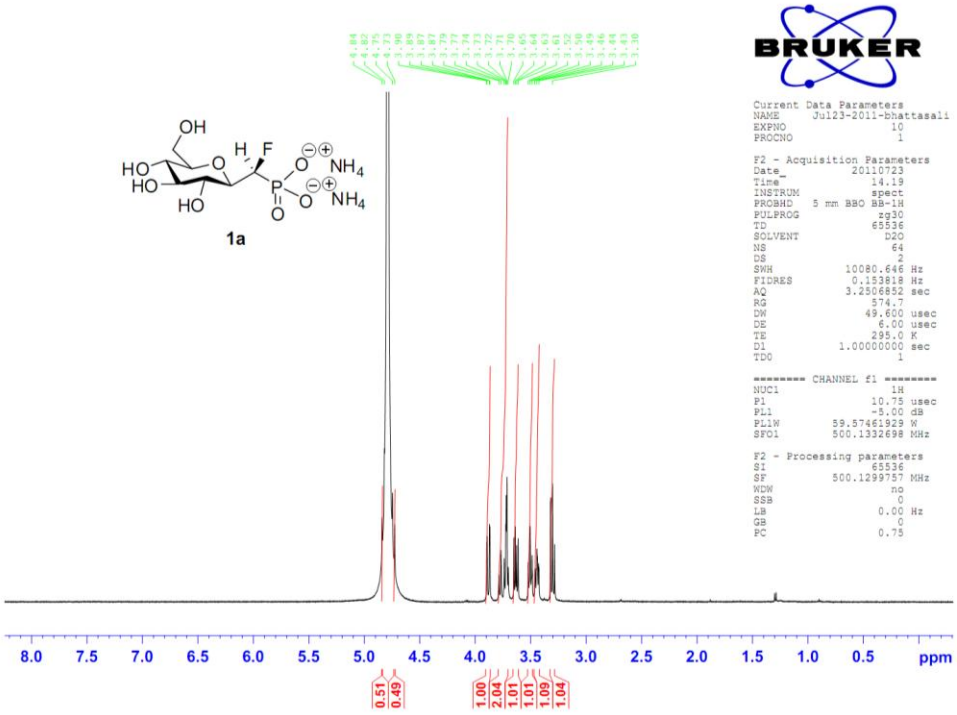

^{1}H NMR spectrum of compound 1a (βG1CF$_S$P).

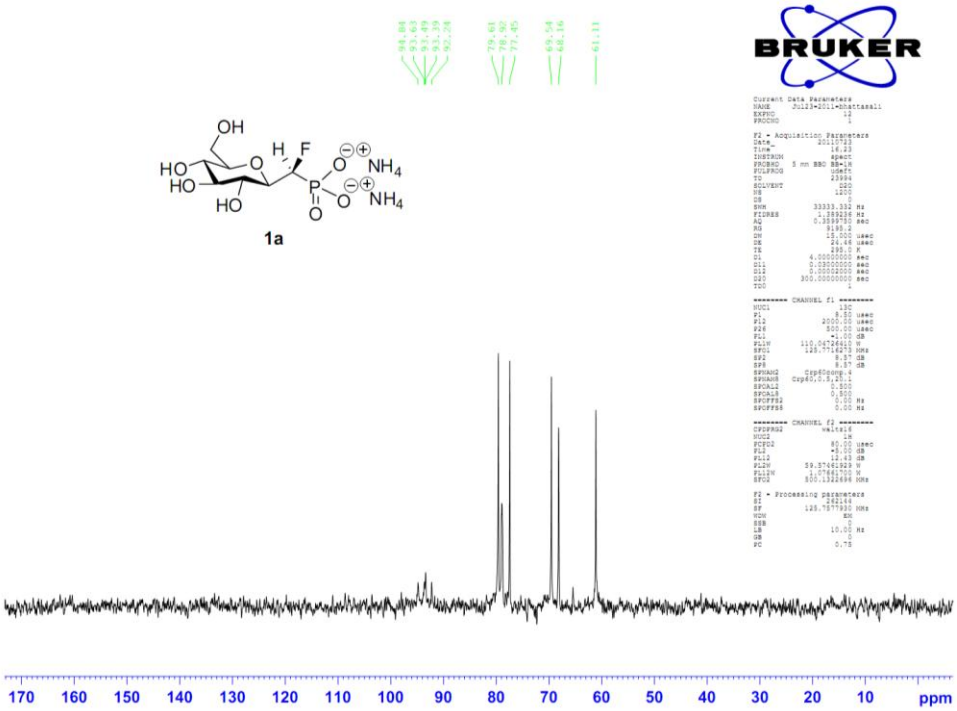

^{13}C NMR spectrum of compound 1a (βG1CF$_S$P).

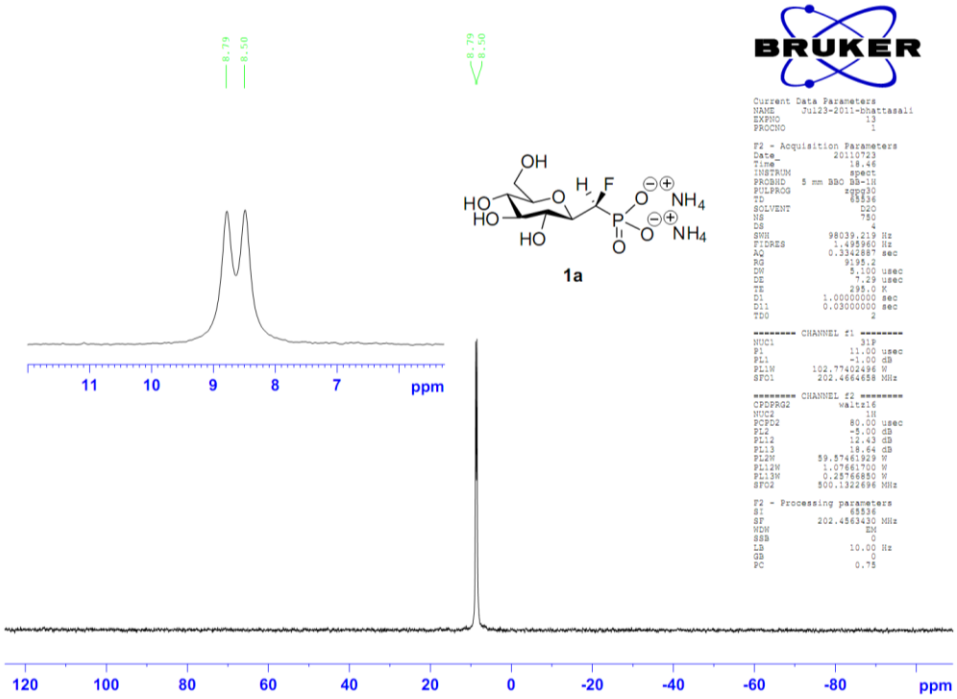

$^{31}P\{^{1}H\}$ NMR spectrum of compound 1a (βG1CF$_S$P).

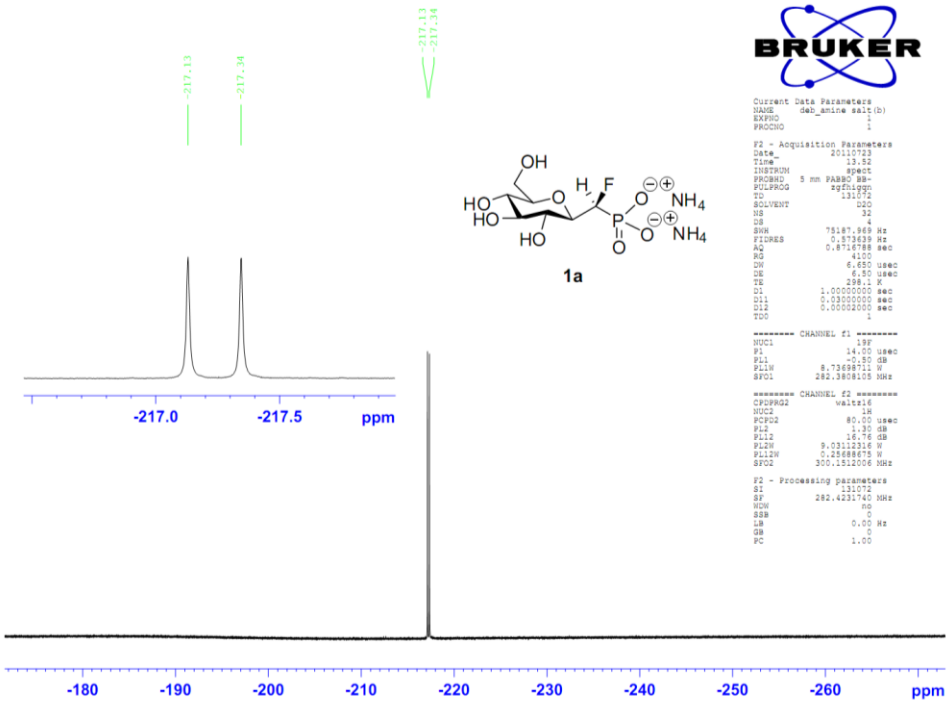

$^{19}F\{^{1}H\}$ NMR spectrum of compound 1a (βG1CF$_S$P).

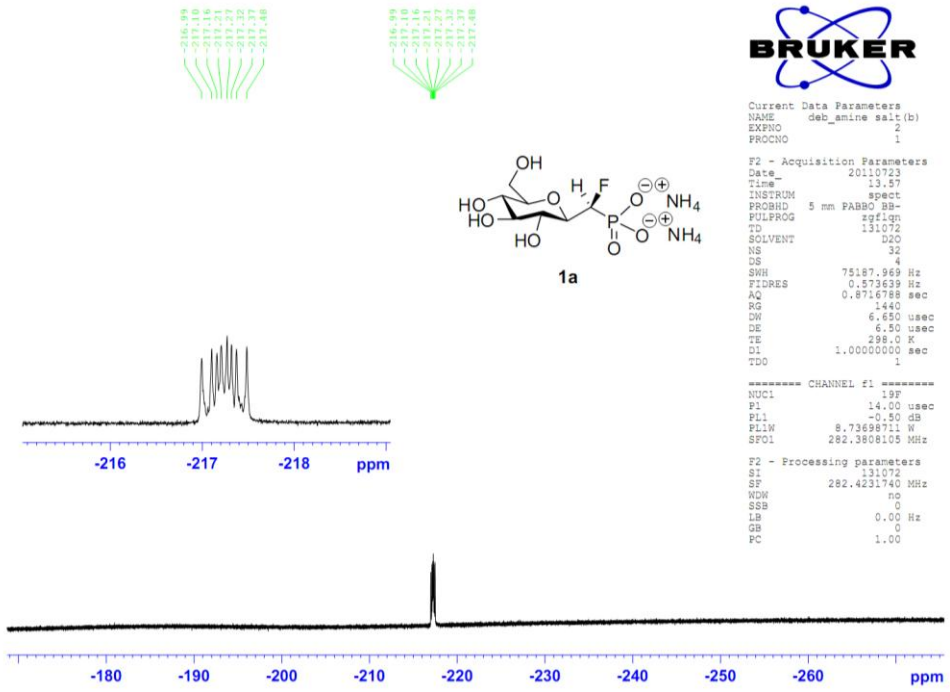

^{19}F NMR spectrum of compound 1a (βG1CF$_S$P).

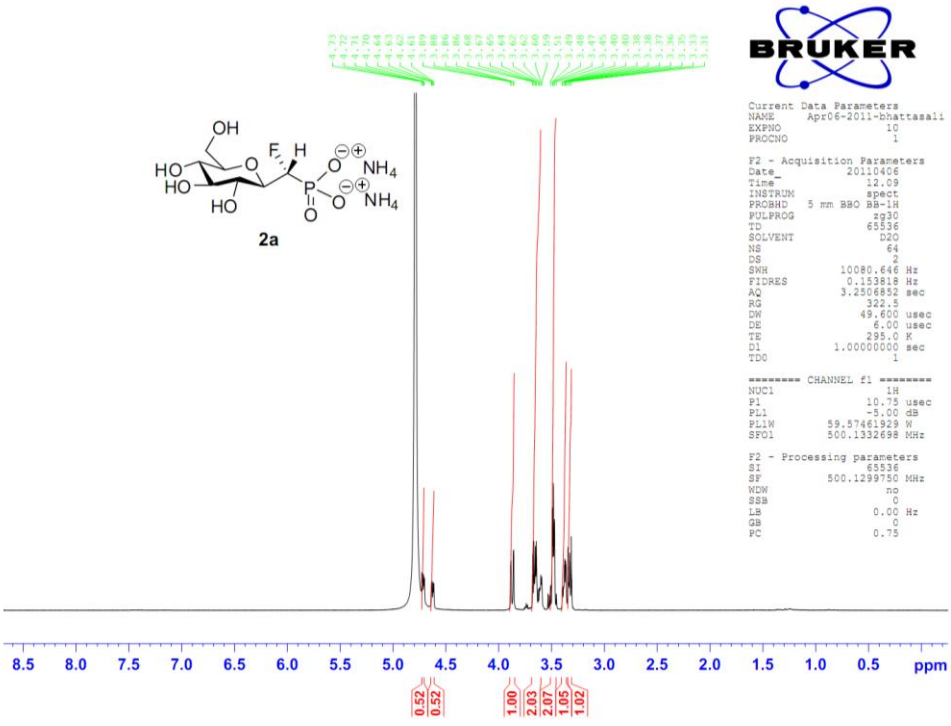

^{1}H NMR spectrum of compound 2a (βG1CF$_R$P).

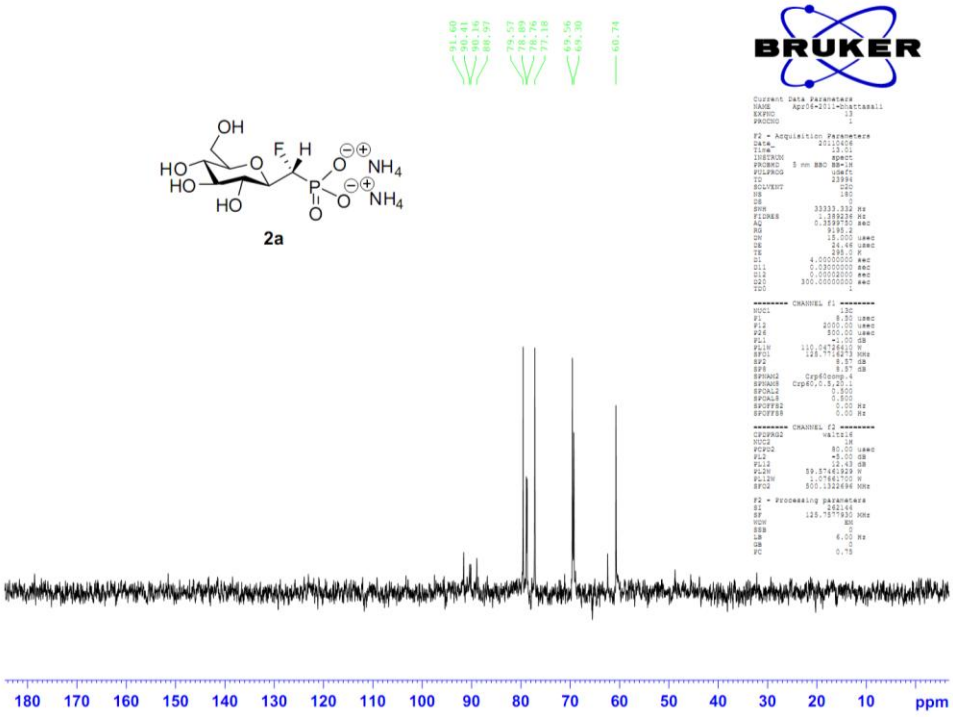

^{13}C NMR spectrum of compound 2a (βG1CF$_R$P).

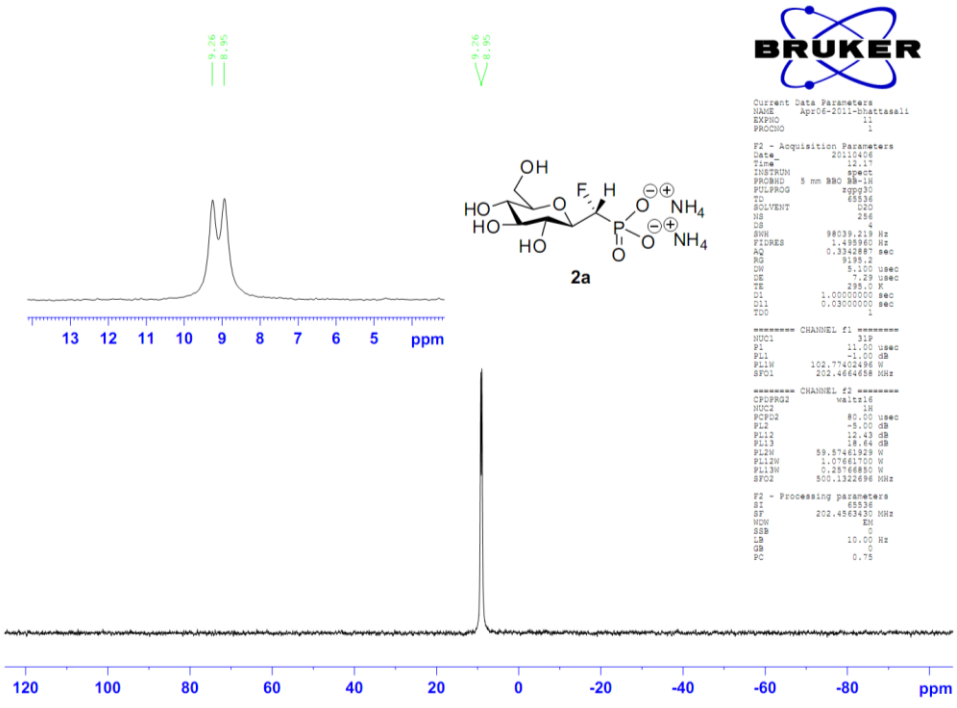

^{31}P{^{1}H} NMR spectrum of compound 2a (βG1CF$_R$P).

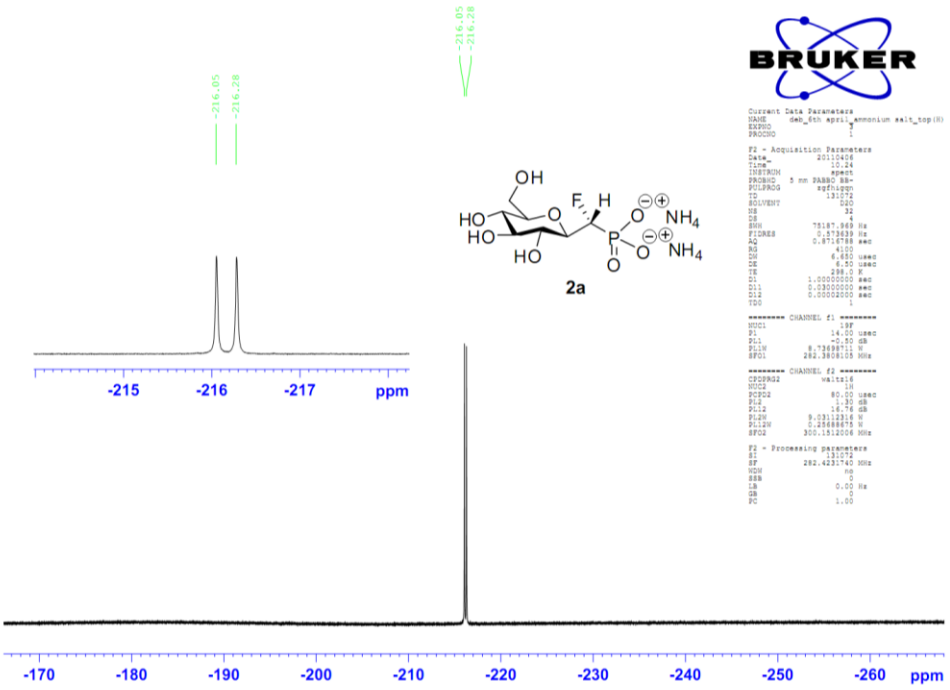

^{19}F{^{1}H} NMR spectrum of compound 2a (βG1CF$_R$P).

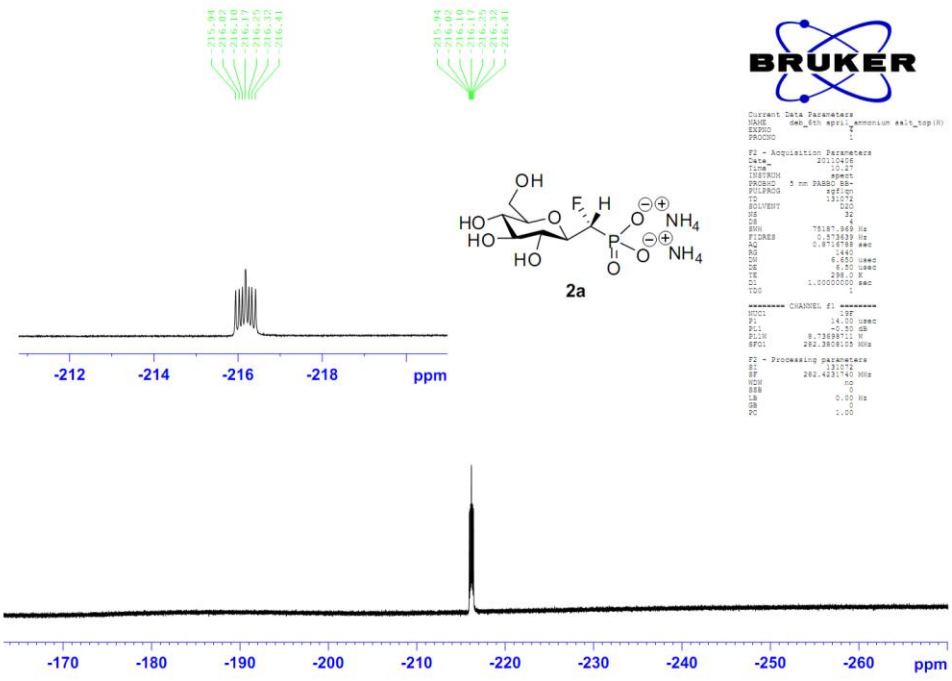

^{19}F NMR spectrum of compound 2a (βG1CF$_R$P).